CrossMark

On the ability of RCMs to capture the circulation pattern of Etesians

Stella Dafka[1] · Andrea Toreti[2] · Jürg Luterbacher[1,3] · Prodromos Zanis[4] ·
Evangelos Tyrlis[5] · Elena Xoplaki[1]

Abstract The Etesians are among the most persistent regional scale wind systems in the lower troposphere that prevail over the eastern Mediterranean during the extended summer season. The performance of five high-resolution EURO-CORDEX regional climate models (RCMs) in simulating the Etesian climatology as well as the associated large-scale atmospheric circulation is investigated. The model outputs are validated against reanalysis datasets (ERA-Interim, 20CR-v2c and ERA20-C) and daily station observations covering the period May to September 1989–2004. Results show that most RCMs coherently reproduce the number of observed Etesian days, the duration of their episodes and the wind field over the Aegean Sea. The majority of RCMs better reproduce in situ wind speed than the driving model, especially over the central and southwestern Aegean Sea. All models represent very well the mean state of the large-scale atmospheric circulation associated with Etesians both at the surface and at mid to upper troposphere, compared to reanalyses. Statistically significant differences vary depending on the subperiod, generally with a better performance for September. The performance of the models improves significantly with decreasing pressure gradient over the Aegean. Finally, results highlight the ability of EURO-CORDEX RCMs in simulating the Etesians over the Aegean, especially the DMI, SMHI and IPSL, which makes them efficient tools for wind energy applications.

Keywords Etesians · Extreme wind · RCMs evaluation · Added value · 20CR-v2c · ERA-20C

✉ Stella Dafka
Styliani.Dafka@geogr.uni-giessen.de

1 Climatology, Climate Dynamics and Climate Change, Department of Geography, Justus-Liebig-University of Giessen, Senckenbergstrasse 1, 35390 Giessen, Germany

2 European Commission, Joint Research Centre, Ispra, Italy

3 Centre of International Development and Environmental Research, Justus Liebig University of Giessen, 35390 Giessen, Germany

4 Department of Meteorology and Climatology, School of Geology, Aristotle University of Thessaloniki, Thessaloniki, Greece

5 Max Planck Institute for Meteorology, Hamburg, Germany

1 Introduction

An important challenge in current climate modeling is the realistic representation of meso-scale features and processes governing the surface wind field (Rummukainen et al. 2015; Salvação et al. 2014; Winterfeldt and Weisse 2009). Indeed, the correct representation of the surface wind field is crucial for a wide range of applications including wind energy (García-Bustamante et al. 2008, 2009), air pollution modeling (Nabat et al. 2015; Menut et al. 2013) as well as climate impact studies (Rummukainen 2010).

The Eastern Mediterranean (EMED) and particularly the Aegean Sea is an area of significant wind energy potential due to the Etesian wind system (Zerefos 1978; Borhan 1998; Bloom et al. 2008; Fyrippis et al. 2010). The Etesians are associated with a persistent low-level northerly flow over the EMED during summer and early autumn, with a maximum during July and August. They are mainly formed by the concurrent occurrence of a persistent high pressure system over central Europe and the Balkans and the extension of the thermal low, prevailing over the Middle East, towards the EMED

(Metaxas and Bartzokas 1994; Tyrlis and Lelieveld 2013; Anagnostopoulou et al. 2014). The name originates from the Greek word, *etesios*, meaning "annual". The Etesians display a strong diurnal variation, reaching their maximum wind speeds usually after noon (12:00 UTC; 15:00 EEST), in response to the daytime deepening of the near-surface thermal low over Turkey (Tyrlis and Lelieveld 2013). Both the dynamics of the Etesians and the related atmospheric circulation are described in detail in Tyrlis and Lelieveld (2013) and Dafka et al. (2016).

The higher spatial resolution of RCMs compared to General Circulation Models (GCMs) results in a better representation of smaller-scale processes, especially in regions with complex orography, land-sea contrast etc. (Rummukainen 2010; Rummukainen et al. 2015). At the same time, RCMs-added value seems to be less relevant at larger spatio-temporal scales (e.g., Diaconescu and Laprice 2013; Feser 2015).

Earlier studies reported that RCMs tend to underestimate strong wind speeds, as well as the number and intensity of storms over Europe (Räisänen et al. 2004; Weisse et al. 2005; Rockel and Woth 2007; Kunz et al. 2010). Rockel and Woth (2007) focused on near-surface wind speed over Europe and identified that most of the RCMs were hardly able to simulate wind velocities above 8 Bft (~17–20 m/s) over land areas during the period 1961–1990. They also showed that models without gust parameterization are not able to realistically capture high wind speeds, in agreement with Schwierz et al. (2009). Kunz et al. (2010) have further shown that RCMs tend to underestimate wind speeds when compared to observations. Lebeaupin-Brossier et al. (2011) and Berthou et al. (2016) found that the increase of spatial resolution allows for a better representation of the strong local winds such as the Mistral over the Gulf of Lions. Obermann et al. (2016) have shown that MED-CORDEX RCMs (including ALADIN and WRF) were able to simulate Mistral and Tramontane events ~74 and 82% of the time, respectively. Further, in most simulations the wind speed was overestimated in valleys and underestimated over the Mediterranean Sea. Although several studies suggested the use of RCMs either for an accurate characterization of wind climates (Pryor and Barthelmie 2011; Iizuka et al. 2012) or for a better representation of the orography and the land surface heterogeneity (Feser et al. 2011; Tölle et al. 2014), the added value of RCMs for wind studies is still under debate. Herrmann et al. (2011) suggested that the added value of the higher resolution is localized in coastal regions and regions of intense winds, such as the Aegean Sea, where the channeling effect of the topography is strong and the representation of the wind speed variability over the whole spectrum is significantly improved. Winterfeldt and Weisse (2009) compared RCM simulations with QuickSCAT satellite and local buoy data over the northeastern Atlantic, as well as the North Sea, and demonstrated that the employment of RCMs

leads to an improved description of wind speed statistics in coastal seas, while conditions in the open ocean were not improved.

To date, only a few analyses on the evaluation of wind speed have been performed based on RCM simulations over the Aegean region. Anagnostopoulou et al. (2014) studied the relationship between large scale circulation and the Etesians over the Aegean Sea for the recent past and the future using RCM simulations carried out with the RegCM3 model. Future projections for the late twentieth century under A1B scenario indicated a strengthening of the Etesians, associated with the strengthening of the anticyclonic action center and a deepening of Asian thermal Low over the EMED. In addition, the majority of previous studies use RCMs in relatively coarse spatial resolutions (25–50 km), while very few focus specifically on the comparison of RCMs with actual measurements from weather stations.

This study aims at evaluating model simulated wind over the Aegean Sea in current climate, using the newest high-resolution EURO-CORDEX RCMs for Europe (Jacob et al. 2014). EURO-CORDEX is the European branch of the Coordinated Regional Downscaling Experiment (Giorgi et al. 2009) and produces ensemble climate simulations based on multiple dynamical and empirical-statistical downscaling models forced by multiple GCMs from the Coupled Model Intercomparison Project Phase 5 (CMIP5; Taylor et al. 2012). The EURO-CORDEX simulations consider the new Representative Concentration Pathways scenarios (RCPs) at an increased spatial resolution of around 12 km (0.11 degrees; EUR-11). This study evaluates the performance of RCMs with respect to the wind field by comparing model simulations with observational datasets and reanalyses. It assesses the added value of RCMs with respect to their driving reanalysis and documents their skill in reproducing the large scale atmospheric circulation associated with Etesians over the Aegean.

The manuscript is organized as follows: in Sect. 2 the data is presented; Sect. 3 gives a description of the methods, while results are presented in Sect. 4. A summary of the main results and the conclusions are presented in Sects. 5 and 6 respectively.

2 Datasets

Simulations from 5 models of the EURO-CORDEX ensemble (see Table S1 in the supplementary material), with different configurations and physical parameterizations, including one meso-scale non-hydrostatic model (WRF-v3.3.1), are used. All models, except ARPEGE-v5.2, are RCMs forced by ERA-Interim (ERAint; Dee et al. 2011) at their lateral boundaries and by sea surface temperature in the interior of the EURO-CORDEX domain. While, ARPEGE-v5.2 is

a global climate model, its temperature, wind speed, and specific humidity is nudged towards ERAint outside the EURO-CORDEX domain. Inside the domain no nudging was applied in any of the models (Prein et al. 2016). ALA-DIN-v5.3 is the same atmospheric model of the CNRM-CM5.1 GCM (ARPEGE-v5.2; Voldoire et al. 2013) just configured on a limited area. Hereafter, all of the models will be characterized as RCMs for sake of brevity. In this study, each model is identified by the name of the institution where the simulation was performed. Simulated mean sea level pressure (SLP), zonal and meridional wind components at 10 m (U10 and V10, respectively), geopotential height at 500 hPa (Z500) as well as zonal wind speed at 200 hPa (U200) for the months May to September and the period 1989–2004, are used to evaluate the present-time wind field.

In addition, daily (at 12:00 UTC) U10 and V10 near-surface wind speeds, SLP, Z500 and U200 from 1989 to 2004 are extracted from ERAint, 20CRv2c (Compo et al. 2011) and ERA20C (Poli et al. 2013) reanalyses. The 20CRv2c is a $2.0° \times 2.0°$ horizontal, 24-layer vertical, 6-hourly global reanalysis covering the period 1851–2012. It assimilates surface observations of synoptic pressure from the International Surface Pressure Databank (ISPDv2.2.4), monthly maps of sea-surface temperature and sea-ice concentration fields from the Hadley Centre Sea Ice and sea surface temperature (SST) data set (HadISSTv1.1). Compared to the previous version 20CRv2, the improved version has more realistic uncertainty in near-surface air temperature and a reduction in spurious centennial trends in the tropical and Polar Regions (Compo et al. 2015). ERA20C is the ECMWF's first atmospheric reanalysis of the entire twentieth century (1900–2010). A coupled atmosphere/land-surface/ocean-waves model is used together with an assimilation system for surface observations including surface pressure and SLP (ISPDv3.2.6 and ICOADSv2.5.1) and surface marine winds (ICOADSv2.5.1). The ERA20C products describe the spatio-temporal evolution of the atmosphere with a 3-hour temporal resolution, on 91 vertical levels, with a horizontal resolution of approximately 125 km. Dafka et al. (2016) evaluated the performance of the 20CRv2 (the former version of 20CRv2c) and the ERA20C in capturing the Etesian wind pattern from 1971 to 2000. The study showed that both datasets provide good representation of the Etesian wind system and the associated atmospheric circulation.

Three-hourly wind speed and direction data from 23 stations over the Aegean Sea and mainland Greece, as well as SLP observational time series for Elliniko and the island of Rhodes are retrieved from the Hellenic National Meteorological Service. The large scale circulation window covers the EURO-CORDEX region i.e. the geographical area from −10W to 37E and 31N to 70N (Fig. 1). Measurements and variables from the instrumental series, reanalyses and models' data are taken at 12:00 UTC, i.e. when the wind is

supposed to reach its highest intensity (Tyrlis and Lelieveld 2013) and cover the extended summer season May to September in the period 1989–2004. Note that the 16-year period is dictated by observational data availability.

3 Methods

3.1 Classification of the Etesians

Following Dafka et al. (2016), we use the pressure gradient over the Aegean Sea to define an Etesian day. The daily (12:00 UTC) SLP difference (ΔP), from May to September, between the stations Elliniko (Attica, PE) and Rhodes (eastern Aegean, PR; Fig. 1) is considered ($\Delta P_{ER} = PE-PR$). In addition, the differences of the closest to the two stations grid points from reanalyses (ΔP_{ERAint}, ΔP_{ERA20C}, $\Delta P_{20CRv2c}$) and each RCM (ΔP_{CNRM1}, ΔP_{CNRM2}, ΔP_{DMI}, ΔP_{SMHI}, ΔP_{IPSL}) regular grids are estimated, respectively. Negative ΔP days indicate southerly flow over the Aegean Sea and thus, are excluded from the analysis. Based on the probability density functions of the estimated ΔP, days with a pressure difference such that median $\leq \Delta P <$ third quartile (Q3) are defined as *moderate Etesian* days; days with a ΔP greater or equal to the Q3 are defined as *intense Etesian* days. Days on which both the simulation/reanalysis and observation agree are classified as *common intense Etesian* days. Finally, an *Etesian episode* is defined as a sequence of two or more consecutive days with $\Delta P \geq Q3$.

3.2 Evaluation metrics

Several assessment criteria are used to evaluate the RCMs, both at surface and in the mid to upper troposphere. Prior to the selection of the intense Etesians, time series of the mean monthly SLP observed at Elliniko and Rhodes are compared to the time series at the nearest grid points for each dataset (RCMs/reanalyses) and tested against trends by using a simple linear regression model combined with ordinary least squares estimation. The monthly mean SLP biases (i.e. differences between the RCMs/reanalyses and the station-based monthly mean SLP at each station) are also computed. Monthly mean values are calculated from the daily observation/value recorded at 12:00 UTC for each month May–September, 1989–2004 and for each dataset. Statistical significance is obtained by applying a two-tailed t test (Wilks 1962). The main characteristics of the classified days are described in terms of the number of intense Etesian days and the frequency of the Etesian episodes. The frequency of the intense Etesian days per subperiod is tested against trend by using a Poisson Regression model (Cameron and Trivedi 1990, 1998). The wind field is evaluated through the comparison of the mean wind speed and the prevailing wind
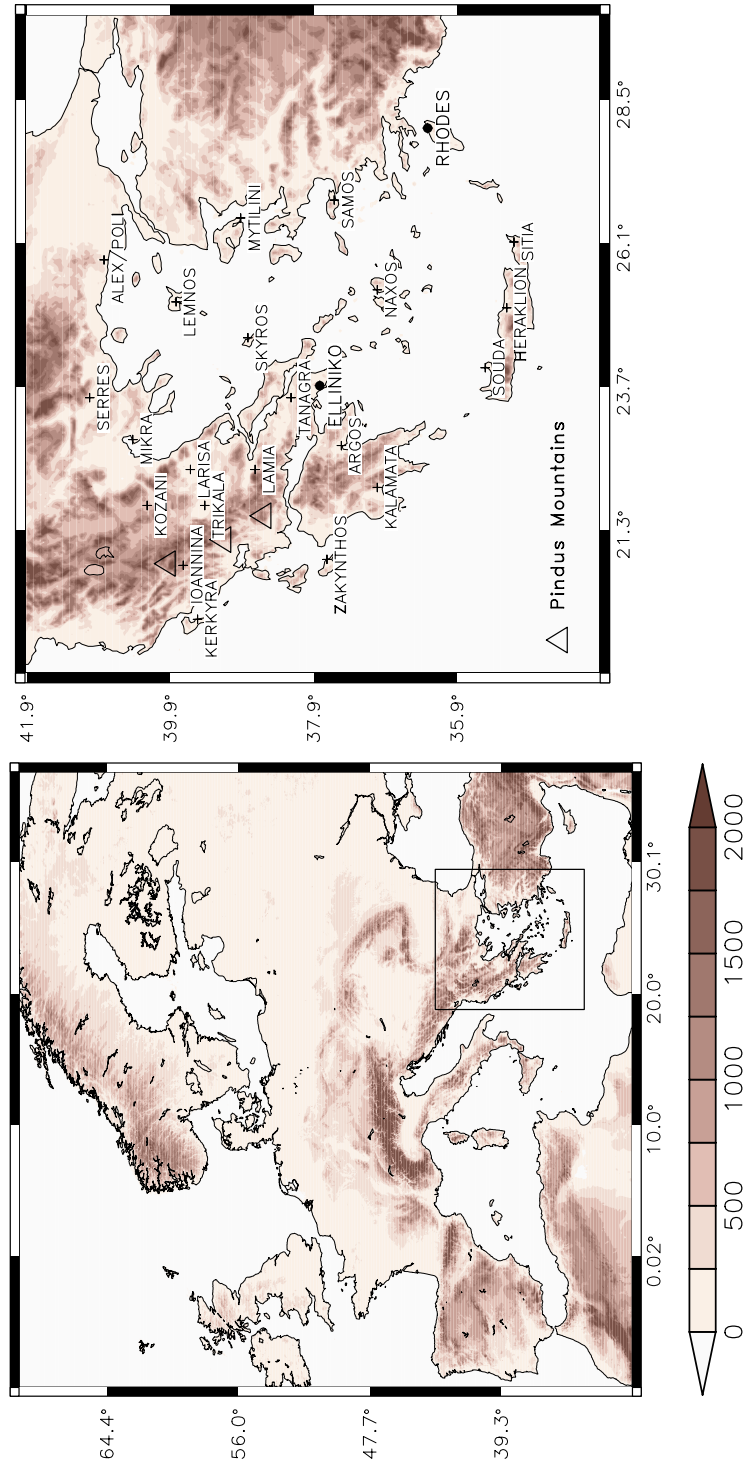
Fig. 1 Left: The EURO-CORDEX domain and the area under investigation delimited by the black box; Right: The study region with the locations of the 23 Greek stations (crosses). Bold dots correspond to the stations of Elliniko and the island of Rhodes. Shading illustrates the orography of the region (in meters). Station time series stem from the Hellenic National Meteorological Service

(wind roses) at several stations. RCMs results are compared to the classified intense Etesian days derived from the time series of observations and reanalyses. The Mean Squared Error (MSE) Skill Score (MSESS) is used to test to what extent the regionally modeled wind better reproduces in situ wind speed than the driving model (ERAint). According to Joliffe and Stephenson (2003), the MSESS is a measure of the skill of the forecast F (here RCM simulated wind speed) relative to a reference forecast R (here ERAint wind speed). It is given by

$$MSESS = 1 - MSE_F / MSE_R.$$

By definition the MSESS can vary between $-\infty$ and $+1$ (forecast exactly matches the observations). Values less than (close to) zero indicate a better (similar) performance of (to) the reference forecast (i.e. ERAint), while positive values indicate an added value of the regionally modeled winds in comparison to the ERAint. The large scale atmospheric circulation related to the classified intense Etesian days is studied by using composite anomaly patterns of SLP, Z500 and U200 from reanalyses fields. The spatial distribution of the 16-year mean May–September differences between the EUR-11 RCMs and reanalyses is then studied. A two-tailed t-test is applied for the assessment of the patterns significance (Wilks 1962). Also note that U200 was available only for DMI, SMHI and IPSL simulations.

For a more comprehensive analysis, the large scale circulation patterns associated with the common intense Etesian days are also studied. In addition, large scale circulation patterns of each variable (SLP, Z500 and U200) associated with moderate Etesians, are analyzed and the surface wind speed biases are computed. Finally, we address the models' performance in stronger and weaker pressure gradient conditions.

The performance of the EUR-11 simulations (in comparison to reanalyses and with respect to the spatial variability of mean SLP and Z500 anomalies as well as the mean wind speed) within the EURO-CORDEX domain and Greece (see Fig. 1) is explored by Taylor diagrams (Taylor 2001) in the period 1989–2004. The Taylor diagram displays multiple information including the spatial correlation, the spatial standard deviation and the centered Root Mean Square Difference (RMSD).

3.3 Regridding

The spatial comparison of the EUR-11 simulations and the reanalyses is carried out by using the coarser grid (i.e. $1.5° \times 1.5°$ for ERAint, $1° \times 1°$ for ERA20C and $2° \times 2°$ for 20CRv2c). In order to compare the RCMs and reanalyses results directly with observations, simulated U10 and V10 are interpolated to observational stations. Such direct validation gives useful estimates of how well RCMs simulate wind locally (Nikulin et al. 2011). In both cases a bilinear interpolation is used. As for the SLP differences, the nearest grid points to the two stations (i.e. Elliniko and Rhodes; see Fig. 1, right panel) are used.

4 Results

4.1 Pressure gradient

This subsection briefly describes results of the mean monthly SLP and the pressure gradient over the Aegean Sea. Both reanalyses and RCMs show a decreasing trend of the mean SLP at the two locations (i.e. Elliniko and Rhodes) in the period 1989–2004 (not shown); however, statistically significant (at the 95% level) is only found in Rhodes for ERAint, CNRM2 and IPSL (~ 1.3 hPa/decade). Statistically positive significant correlations (~ 0.8–0.9) can be found between the station-based mean SLP and the RCMs and reanalyses for both sites. The estimated monthly SLP biases show that reanalyses and RCMs realistically reproduce the pressure tendencies at both stations. Statistically significant positive (negative) biases ~ 1–1.5 hPa (~ 1–1.5 hPa) are calculated for ERA20C (IPSL) at both stations.

In order to assess the ability of the RCMs to capture the pressure gradient over the Aegean Sea, the simulated SLP differences of reanalyses (ΔP_{ERAint}, ΔP_{ERA20C}, $\Delta P_{20CRv2c}$) and model simulations (ΔP_{CNRM1}, ΔP_{CNRM2}, ΔP_{DMI}, ΔP_{SMHI}, ΔP_{IPSL}) are compared with the observed ΔP_{ER} (Fig. S1 in the SOM). The comparison shows similarities on the first quartile and the median of the distribution. However, CNRM2 shows a smaller interquartile range, while CNRM1 overestimates the maximum compared to the station time series. Both SMHI and DMI overestimate the third quartile and the median of the distribution. 20CRv2c shows the smallest interquartile range, while it underestimates the maximum, the third quartile and the median of the distribution. The ERA20C and IPSL reproduce well the SLP differences of observed data (Fig. S1 in the SOM).

4.2 Classified Etesian days

We provide results for the extreme wind events (i.e. intense Etesians) as classified by using the individual simulations, observational series and reanalyses. Around 20–23% of the May–September days of each dataset are classified either as intense or moderate Etesians, while around 15% show negative pressure differences, implying a southerly flow over the Aegean (Table 1). The 20CRv2c underestimates the frequency of the southerly winds (~ 7%) while IPSL overestimates their frequency (~ 21%). Figure 2 shows the monthly number of intense Etesian days, in each dataset and the percentage of common intense Etesian days between RCMs/reanalyses and the station series. The average number of intense

Table 1 Classification of days for the extended summer season May to September in the period 1989–2004

Condition	Name of group	Percentage of days (mean of all datasets)
$\Delta P < 0$	Southerly flow	14.7%
$0 \leq \Delta P <$ Median	Non Etesians	42.4%
Median $\leq \Delta P < Q_3$	Moderate Etesians	21.4%
$\Delta P \geq Q_3$	Intense Etesians	21.5%
Percentage of simulated intense Etesian days that agree with the observed	Common intense Etesians	80% Reanalyses 50% RCMs

Fig. 2 Number of intense Etesian days in the period May–September, 1989–2004 (upper panel). Discontinuities in the lines imply that the number of intense Etesian days is zero. Percentage of *common* intense Etesian days is shown in the lower panel
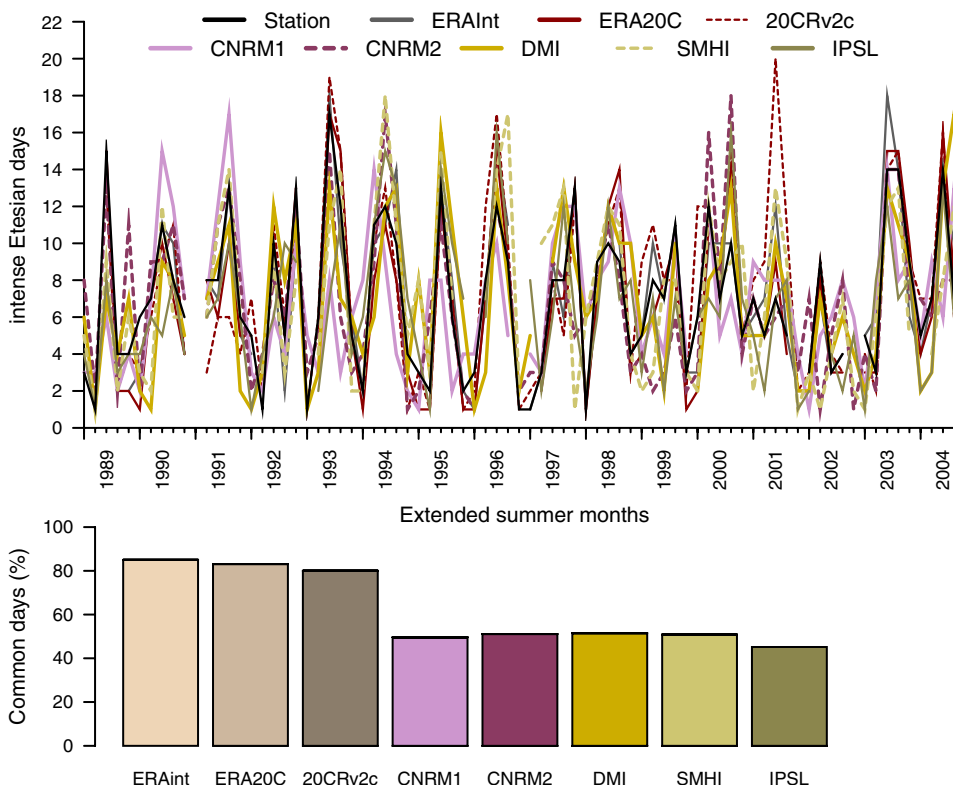
Etesians is 33 days per dataset and for each extended summer season. ERAint and ERA20C seem to perform slightly better than the 20CRv2c in the temporal evolution of intense Etesian days over the period 1989–2004. The monthly correlation between the number of the station-based and the ERAint-, ERA20C- (20CRv2c-) based intense Etesian days is 0.9 (0.8). RCMs (with the exception of IPSL) show good skill in the simulation of the number of intense Etesian days compared to station series, with an average underestimation of 4% or 20 days (11% or 60 days) over the period 1989–2004. However, the monthly correlation is rather low (~ 0.6). Higher consistency between the RCMs and the station time series is found only during the last 5 years (2000–2004) considering the total number of intense Etesian days over the extended summer period (not shown). RCMs also capture the Etesians "collapse" observed in 2002 (Tyrlis

et al. 2015). It is worth noting that 80% (50%) of the intense Etesian days classified in the two reanalyses (RCMs) correspond to those classified in the station series (Fig. 2; lower panel). Overall, RCMs give the correct number of days that fall into each class, while they are able to correctly simulate the intense Etesian days ~ 50–60% of the time (Table 1).

The trend analysis on the frequency of the intense Etesian days over the period 1989–2004 (not shown) reveals statistically significant changes (p-value ≤ 0.05). A significant annual increase of around 9% and 5% is estimated in all reanalyses for May and June. As for the RCMs, CNRM2 shows an annual increase of 5% in May and an annual reduction of 7% in September. A significant increase of Etesians at the beginning of the summer (May and June) and evidences for less frequent Etesian episodes in September have been also identified by previous studies

(Tyrlis and Lelieveld 2013; Dafka et al. 2016). Furthermore, both reanalyses and the RCMs show good skill in simulating the monthly frequency of Etesian episodes (especially the CNRM2, not shown). All RCMs, but IPSL, are able to capture episodes that are persistent beyond the typical synoptic time scale (longer than 5–6 days), potentially meaning that RCMs reproduce the mid-latitude dynamics leading to prolonged episodes. SMHI tends to overestimate episodes' duration, which is also consistent with the overestimated pressure gradient over the Aegean (Fig. S1 in the SOM).

4.3 Wind speed

The performance of the EUR-11 simulations with respect to the spatial variability of mean wind speed at grid-point scale is assessed by comparing the simulated wind speed against the observed one at the 23 Greek stations and the reanalyses over the period 1989–2004 (Fig. 3). During intense Etesian days, the observed mean wind field at the stations (Fig. 3a) presents higher wind speed over the Aegean Sea compared to mainland. The standard deviation is ~2 m/s at each station. Highest mean wind speed values are found over central (11.1 m/s in Naxos) and southern (10 m/s in Sitia,
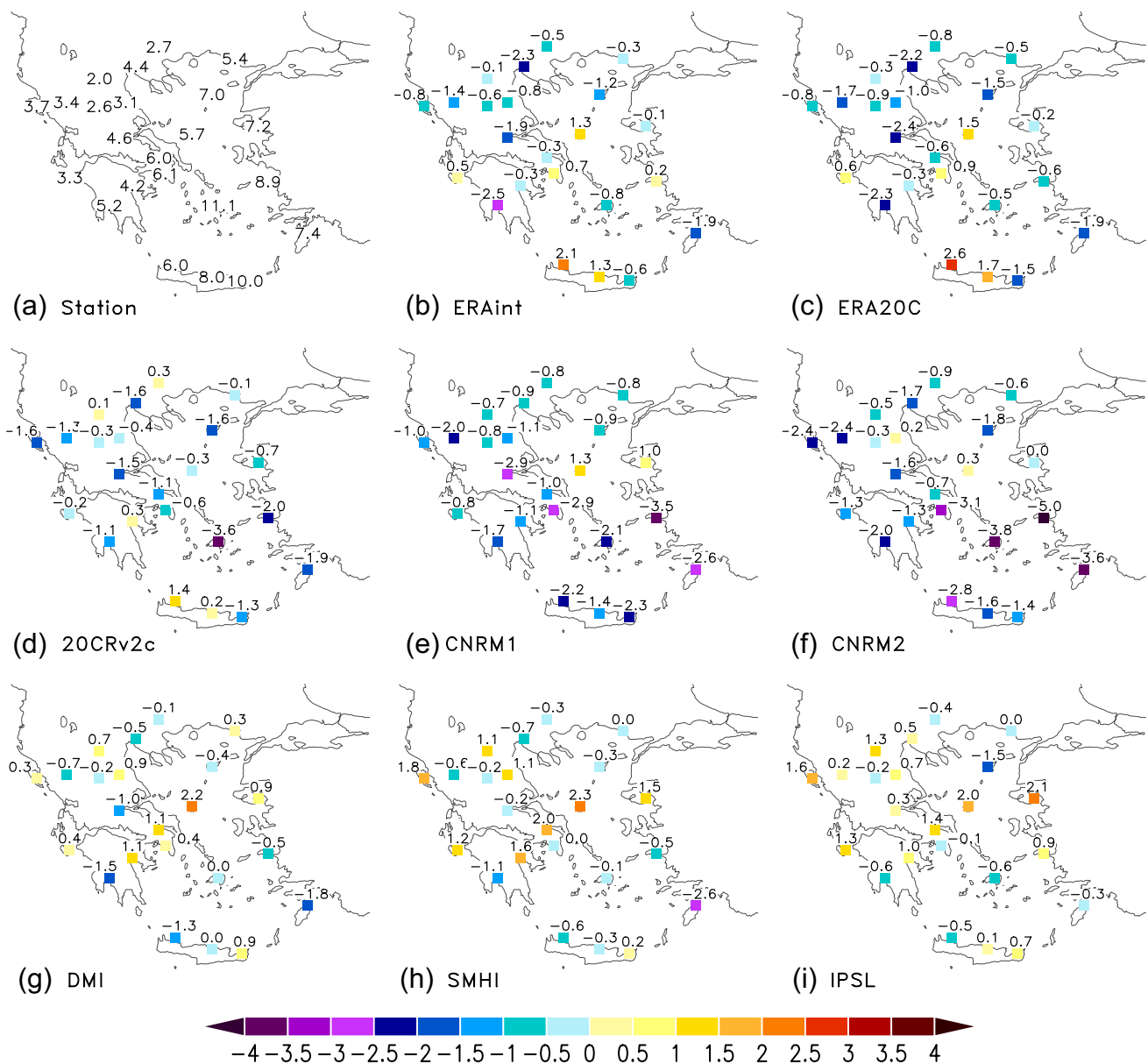

Fig. 3 Mean wind speed biases (m/s) during the intense Etesian days of **b–d** the reanalysis products (reanalysis minus station) and **e–i** the EUR-11 simulations (RCM minus station) over the period 1989–2004. The upper-left panel (**a**) shows the observed mean wind speed at stations

Crete) Aegean Sea. The three reanalyses underestimate near-surface wind speed (especially the 20CRv2c), with wind speeds ~ 1–1.3 m/s lower than the observations (exceptions are Heraklion and Souda, Crete and a few more other stations; Fig. 3b-d). Kent et al. (2013) and Jones et al. (2016) have also shown that reanalyses underestimate near-surface wind speed, especially at high wind speeds and in coastal regions.

Regarding the models, CNRM1 and CNRM2 (hereafter CNRMs) generally underestimate the mean wind speed at most stations (Fig. 3e, f). The larger underestimation is observed over the Aegean Sea, exceeding 3–5 m/s in some cases, which is consistent with the underestimated pressure gradient over the Aegean (see Fig. S1 in the SOM). The SMHI and DMI models show a good representation of the intense Etesians wind speed (Fig. 3g,h). The averaged biases over the Aegean are ~ 0.8 m/s. IPSL, despite the underestimation of the mean SLP of Elliniko and Rhodes (see Sect. 4.1), provides very good results in terms of wind intensity; however, the mean wind speed over continental Greece is generally overestimated (Fig. 3i).

The MSESS (Fig. 4) is applied to estimate added value of the regionally modeled wind with respect to ERAint over the Aegean. CNRM1 does not add any value almost throughout the domain (Fig. 4a); CNRM2 adds value in wind speed in north and central Greece (Fig. 4b). The other RCMs show distinct added value along the slopes of Pindus mountainous range (Fig. 4c–e). In addition, DMI, SMHI and IPSL perform better than the forcing reanalysis over the southwestern Aegean coastal stations, which are located under the Etesian wind influence (Fig. 4c–e). Higher positive values, which indicate a better representation in the RCMs, are found in Elliniko, Naxos, Heraklion and Souda (Fig. 4c–e). However, no added value is found over the eastern Aegean coasts, (Fig. 4), indicating that the complex topography and coastline effects in this region are not resolved properly by the models.

4.4 Wind direction

A complementary study of the 10-m wind direction has been performed at eight coastal stations, under the Etesian wind influence over the Aegean. We compared wind roses (at 12:00 UTC) obtained from RCMs, reanalyses as well as observations for the intense Etesians as identified in each dataset (Fig. 5). All datasets reproduce adequately
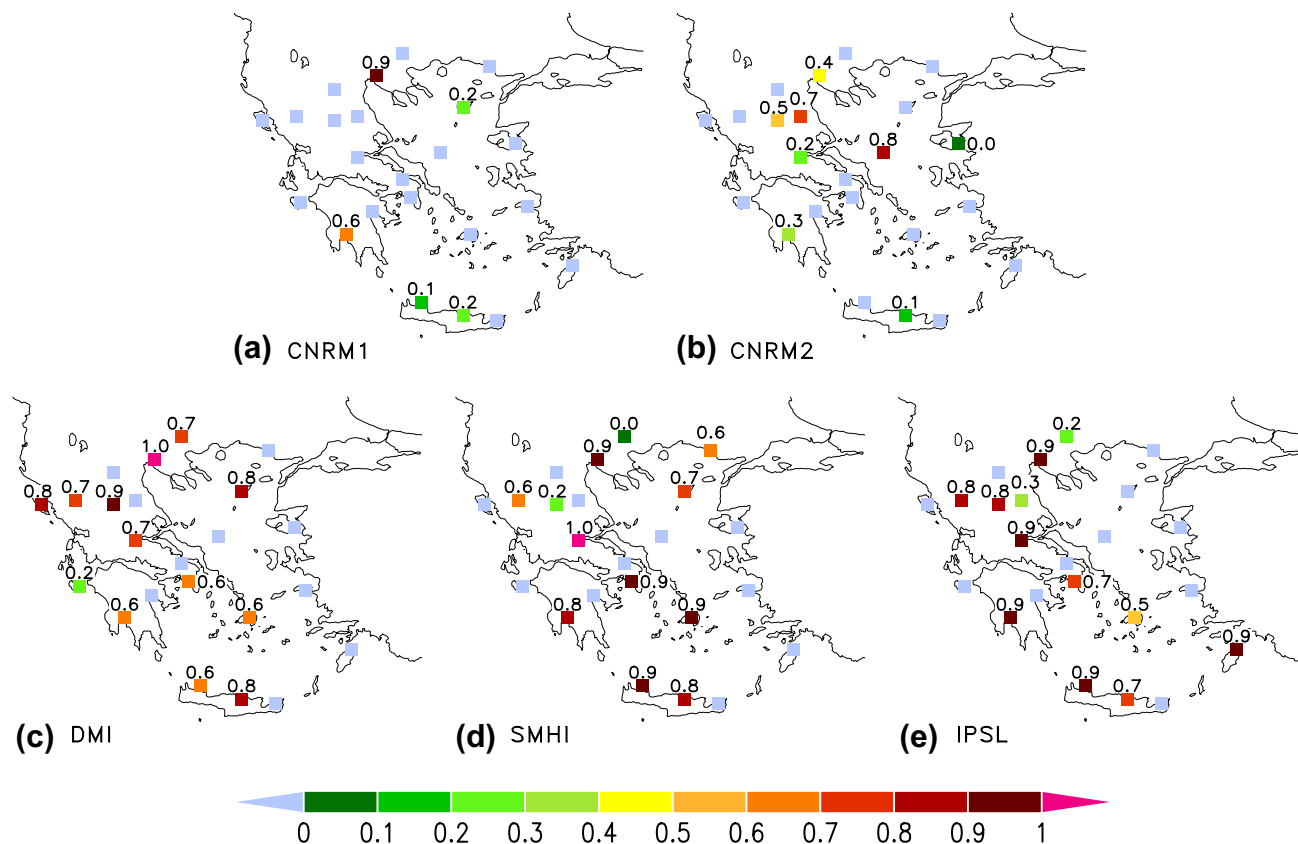

Fig. 4 MSESS of the mean wind speed of the intense Etesian days for the period 1989–2004 at the 23 stations, using ERAint as reference and each RCM (**a**–**e**) as forecast. Reddish (bluish) colors indicate an (no) added value of the regionally modeled winds in comparison to ERAint
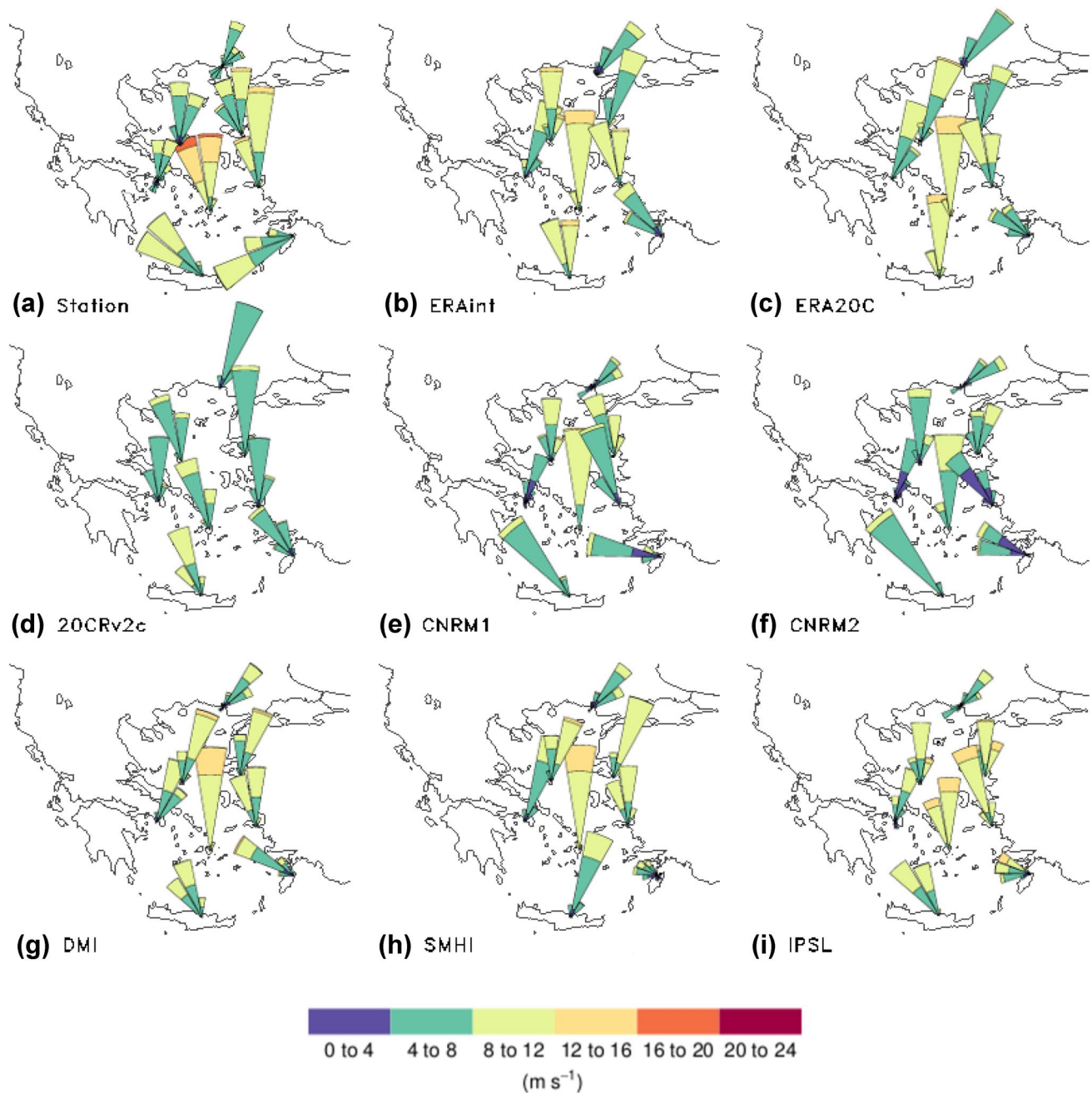
Fig. 5 Wind roses at eight sites over the Aegean Sea during May–September 1989–2004. Observations of wind direction are binned into 12 cardinal directions. The bins are sized according to the proportion of the frequency of measurements

the Etesian wind pattern (Kotroni et al. 2001). As shown in Fig. 5, the Etesians blow predominantly from a northeasterly direction over the northern Aegean (Alexandroupoli, Skyros, Mytilini), northerly over the central Aegean (Naxos) and northwesterly along the south-eastern coasts (Heraklion and Rhodes respectively). However, neither reanalyses nor models (Fig. 5b–i) are able to simulate the dominant southwesterly winds at Rhodes (Fig. 5a). During summer, local scale circulation phenomena such as sea-land breezes can develop

due to the differential heating of land and the adjacent water surfaces. For instance, Elliniko and Alexandroupoli (Fig. 5a) are characterized by south-southwesterly winds, associated with lower speed, which could be related to the development of sea-breeze circulations (Kallos et al. 1993; Pezzoli 2005). Nevertheless, reanalyses cannot capture the development of such local circulation systems (Fig. 5b–d) and therefore are not able to realistically reproduce the wind direction variability at these stations. It seems that the coarse resolution

has negative impact on the reanalyses performance over the Aegean basin. In addition, wind speed is clearly underestimated in 20CRv2c (Fig. 5d).

CNRMs show a consistent tendency to underestimate the wind speed; however they show better skill in simulating the details and the pattern of the wind direction, introduced by the spatial heterogeneity of the Aegean basin, compared to the reanalyses, reflecting clearly the sea breeze in Alexandroupoli (Fig. 5e, f). Despite of a slight overestimation of the wind speed, the wind direction distribution tends to be more similar to the observed one in DMI and SMHI, however the southerly flow associated with the sea breezes is not simulated (Fig. 5g, h). IPSL shows not only similarities to observational measurements in terms of wind speed but also captures the regional variability of wind directions (Figs. 4, 5e).

4.5 Large scale atmospheric circulation and Etesians

SLP, Z500 and U200 daily anomalies (with respect to May–September in the period 1989–2004) are calculated. The large scale atmospheric circulation is studied by using SLP, Z500 and U200 composites of anomaly differences between the EUR-11 simulations and the reanalyses. A two-tailed t test is applied for the assessment of the patterns significance. As patterns against ERA20C and 20CRv2c (Figs. S2–S9 in the SOM) show consistency with those of ERAint, only the latter are shown. In addition, due to the pronounced differences of the Etesian episodes for each month (Tyrlis and Lelieveld 2013; Dafka et al. 2016) the extended summer season is divided in four distinct subperiods: May (M), June (J), July–August (JA) and September (S).

4.5.1 SLP anomaly differences

Figure 6 provides an overview of the spatial SLP anomaly differences between the EUR-11 simulations and the ERAint for the intense Etesian days. The top row (Fig. 6a–d) shows the SLP anomaly composites of ERAint associated with the intense Etesian days. The evaluation indicates a reasonably well representation of the spatial SLP variability (Fig. 6). In all RCMs the SLP large-scale pattern is well reproduced and differences typically do not exceed 1.5–2.5 hPa and are pinpointed mostly close to the outflow boundary (Fig. 6).

More specifically, CNRMs show a statistically significant underestimation of the mean SLP anomalies (0.5–1 hPa) over the south-eastern Balkans and western Turkey in the period July–September (Fig. 6g, h, k, l; more pronounced in September for CNRM1). These centers spatially coincide with the position of the high and low pressure system associated with the Etesians (see Fig. S2 in the SOM). Indeed, both RCMs show a weakening (intensification) of the high (low) pressure system over the southern Balkans (Aegean

and Turkey), which is likely connected with the underestimation of the wind speed over the Aegean Sea (Fig. 3d, e). An annual reduction of the intense Etesian days is found in September but only for CNRM2 (see Sect. 4.2).

All models in May and June produce a statistically significant overestimation of the mean SLP anomalies particularly over central and eastern Europe (Ukraine) and the Balkans (Fig. 6e, f, i, j, m, n, q, r, u, v), with maximum values of around 3–4 hPa in May (Fig. 6e, i, m, q, u). This pattern is also identified, although less pronounced, during July–August for DMI, SMHI and IPSL (Fig. 6o, s, w). This overestimation potentially leads to a stronger anticyclonic center over the Balkans. SMHI shows also an intensification of the low pressure system in the period June to September (Fig. 6r–t), which is consistent with the overestimated pressure gradient over the Aegean (see Fig. S1 in the SOM). Strandberg et al. (2014) also reported the positive anomaly (1–2 hPa higher than in ERAint) for the SMHI over the southern Balkans in summer. However, the small biases imply a realistic representation of the large scale circulation in SMHI. In addition, our study shows that there is no considerable impact in the ability of SMHI to capture near-surface winds. Indeed, biases in 8 out of 11 stations over the Aegean Sea are less than 0.5 m/s respectively (Fig. 3h).

4.5.2 Z500 anomaly differences

The Z500 anomaly composites of the intense Etesian days, derived from the reanalyses, are characterized by two configurations depending on the investigated subperiod (see Fig. S3 in the SOM). A quadrupole-type 500 hPa height anomaly pattern is identified in May and September. It consists of (i) a negative anomaly center over the Atlantic, (ii) a broad area of positive anomalies extending over western, central and northern Europe, (iii) an anomalous trough extending from the Barents Sea towards Eastern Europe and the EMED, and (iv) an anomalous ridge stretching from the Siberia towards the Caspian Sea. However, in July–August only the intermediate dipole (less pronounced) is identified; while June seems to be a circulation period between the two atmospheric configurations. The pattern in May and September is related with the mechanism described in Tyrlis and Lelieveld (2013). They proposed that both the timing of the Etesians onset and their duration are influenced by the mid-latitude dynamics. As aforementioned, the wave disturbances, originating over the North Atlantic, activate the development of a strong ridge over the Balkans, which in turns induces a strong pressure gradient over the Aegean.

Figure 7 provides an overview on the mean spatial Z500 anomaly differences between the EUR-11 simulations and the ERAint for the intense Etesian days. The top row (Fig. 7a–d) shows the Z500 anomaly composites of ERAint associated with the intense Etesian days. The spatial patterns
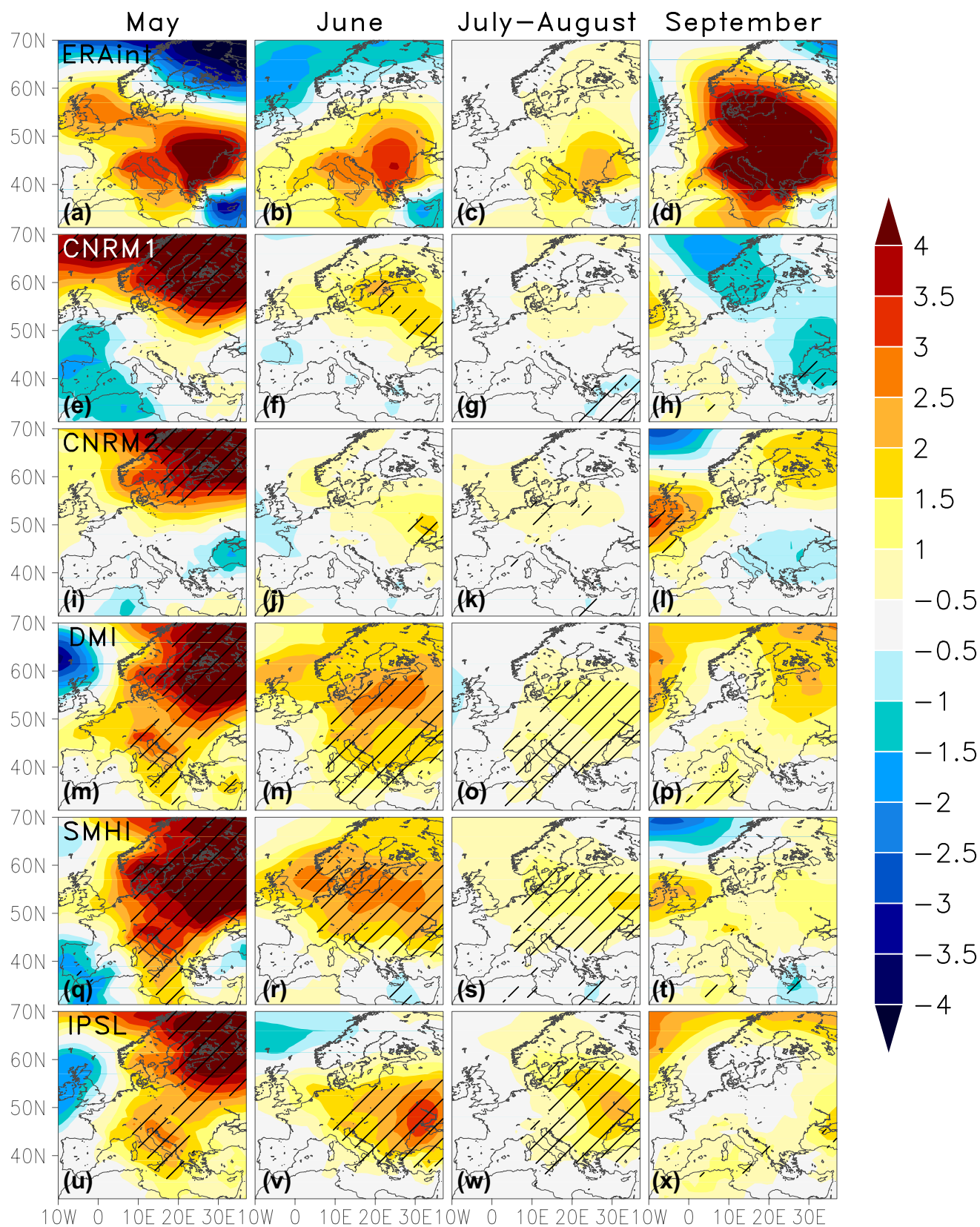
Fig. 6 Mean SLP (hPa) anomaly composites of (**a–d**) ERAint and differences between the (**e–h**) CNRM1, (**i–l**) CNRM2, (**m–p**) DMI, (**q–t**) SMHI, (**u–x**) IPSL and the ERAint for each subperiod (M,J,JA,S) during the intense Etesian days. SLP anomalies are calculated with respect to the extended summer season of the period 1989–2004. Hatching denotes statistically significant areas at the 95% level
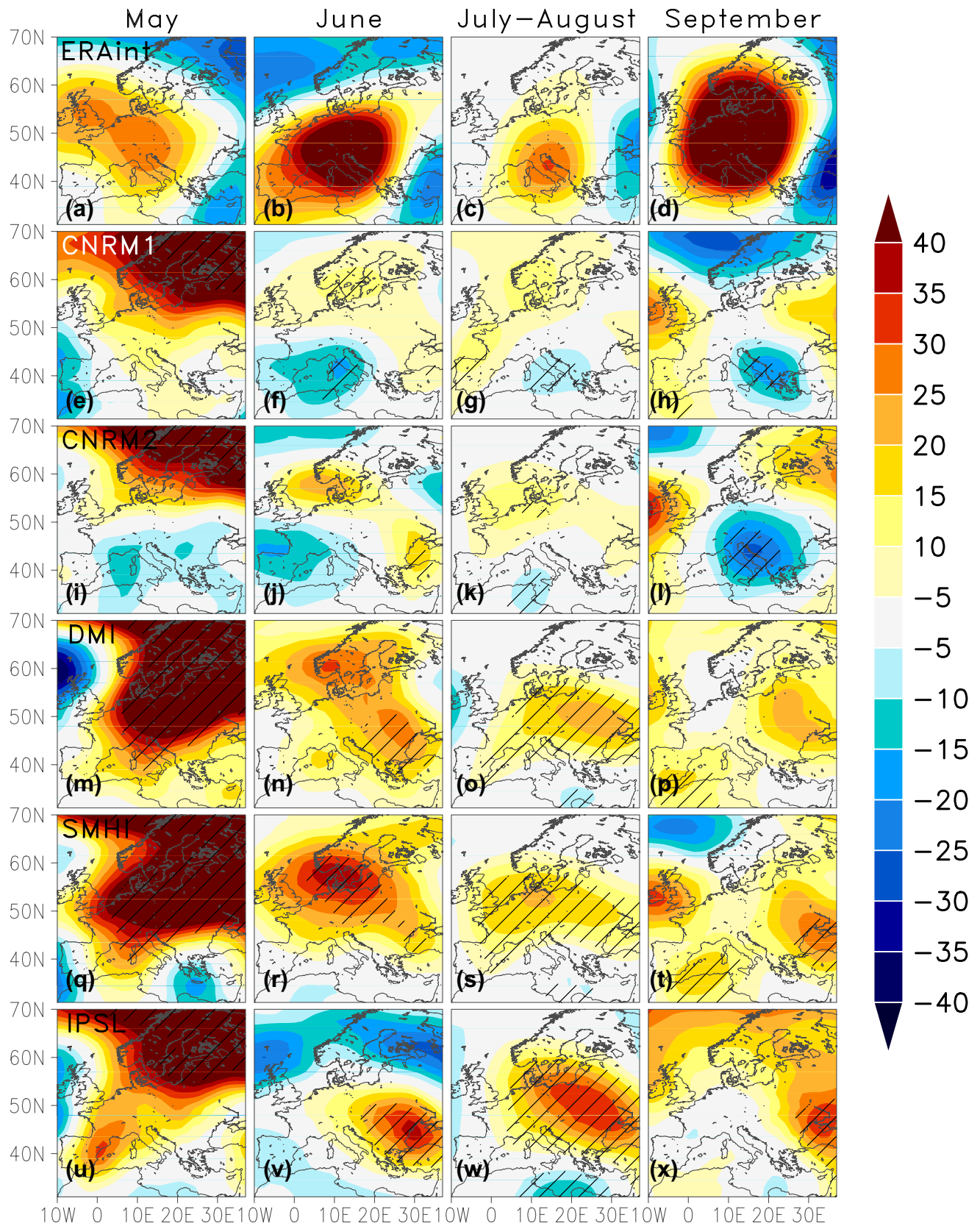
Fig. 7 As Fig. 6 but for Z500. Values in gpm

of statistically significant differences are consistent with the ones at surface (Fig. 6). A good agreement between RCMs and ERAint is found, as statistically significant differences do not exceed 10–30 gpm in most of the EURO-CORDEX domain (Fig. 7). However, this is not the case in May, where all models show a statistical significant overestimation of the mean Z500 anomalies (~70 gpm; Fig. 7e, i, m, q, u), which covers much of the European continent for DMI, SMHI and IPSL (CNRMs). DMI, SMHI and IPSL show a statistically significant overestimation of about 30–40 gpm over south-eastern Europe in the period June to September (Fig. 7n–p, r–t, v–x). This pattern is also identified, although less pronounced, in June for CNRM2 (Fig. 7j). The mean 500-hPa circulation during June to September (not shown) features an amplified anomalous ridge in the west, extending from central Europe to the Black Sea, and a weaker trough in the east, compared to the ERAint. Such a configuration is connected with a shallower anomalous meridional circulation in the upper mid-troposphere that may block somehow the intrusions of cold air masses towards the Aegean Sea and thus, the northerly flow (Etesians) over the Archipelago (see Sect. 4.2). This phenomenon is especially strong in June for IPSL. It is worth to mention that the IPSL identifies ~30 days less in June over the 16 year period, compared to ERAint and station series. Nevertheless, DMI, SMHI and IPSL show low wind speed biases over the Aegean (~0.8 m/s, Fig. 3g–i) and not a clear underestimation, as expected due to the weaker anomalous meridional circulation in the upper mid-troposphere. This could imply that, biases do not result from circulations internal to the domain generated by the model, but from weaknesses/limitations in the wind speed representation scheme. On the other hand, although the CNRMs perform better in reproducing the SLP and Z500 patterns compared to other models (Figs. 6, 7e–l), they strongly underestimate the wind speed at 10 m (especially over the Aegean; Fig. 3e, f).

4.5.3 U200 anomaly differences

RCMs shortcomings in the surface wind representation usually arise either due to the effects of the large scale biases in the free atmosphere or due to the unresolved detailed regional processes in the boundary layer. Etesians are strongly influenced by the position of the Subtropical and Polar Jet stream (STJ and PJ respectively; Dafka et al. 2016). Figure 8 provides an overview on the mean spatial U200 anomaly differences between the aforementioned simulations and the ERAint for the intense Etesian days. The top row (Fig. 8a–d) shows the U200 anomaly composites of ERAint, associated with the intense Etesian days. A good agreement between RCMs and the driving reanalysis has been found in each subperiod (except May), indicating their ability to capture the position and strength of the jet

streams. However, the IPSL in June to September shows a statistically significant overestimation of the mean U200 anomalies over the northwestern part of the Black Sea region (at 45–50°N and 28°E; Fig. 8j), which is also clearly seen in September, north of the British Isles, for SMHI (Fig. 8l). This might indicate a southward displacement of the PJ in comparison to the ERAint. Such a displacement, which is usually evident during the peak period (Dafka et al. 2016) can lead to merging with the STJ and thus to very strong synoptic scale descending motions and subsidence over the Aegean Sea. In addition, all models, in the period June to September, slightly underestimate the mean U200 anomalies (~2–4 m/s) over the Balkans and Turkey (Fig. 8f–h, j–l, n–p; more pronounced in the peak period, July–August), indicating an underestimation of the STJ. Similarly here there is no impact in surface wind speed, as models do not show a clear underestimation of the wind speed over the Aegean due to the STJ's underestimation.

To sum up, results regarding the large scale atmospheric circulation patterns and intense Etesians (Sects. 4.5.1, 4.5.2, 4.5.3) revealed a good agreement between models and reanalyses (except in May). Best results are obtained with the CNRMs in each subperiod (Figs. 6, 7e–l) and for all models in September (Figs. 6, 7 h, l, p, t, x). Further, all RCMs captures the jet streams, with the most notable difference being the weaker negative U200 anomalies over the Balkans and Turkey. Finally, it seems that the shortcomings of the low to mid and upper-level atmospheric circulation are inherited to a small extent in surface wind speed.

Large scale atmospheric circulation patterns of the common intense Etesians days are almost identical to those associated with the intense Etesian days (not shown). The most notable differences are the slightly improved large scale circulation (both the SLP and Z500 anomalies) in May and the better representation of the jet streams in each subperiod, when only the common intense Etesian days are considered. Quite interesting is that, in some cases, RCMs perform better when all intense Etesians are taken into account (e.g., the SLP anomalies differences are found smaller in the period July to September for the CNRMs; not shown). This may indicate that the overall skill of RCMs is good and it is not confined only during the days that both simulations and observations agree (i.e. during the common intense Etesian days).

To assess the performance of RCMs with respect to the pressure gradient over the Aegean, we consider also the moderate Etesian days. Results indicate that both the SLP and Z500 anomaly differences are substantially reduced and a better agreement in the simulation of the jet streams is achieved. The best agreement with ERAint is found during the period July to September (May to August) for the DMI, SMHI and IPSL (CNRMs). The wind speed
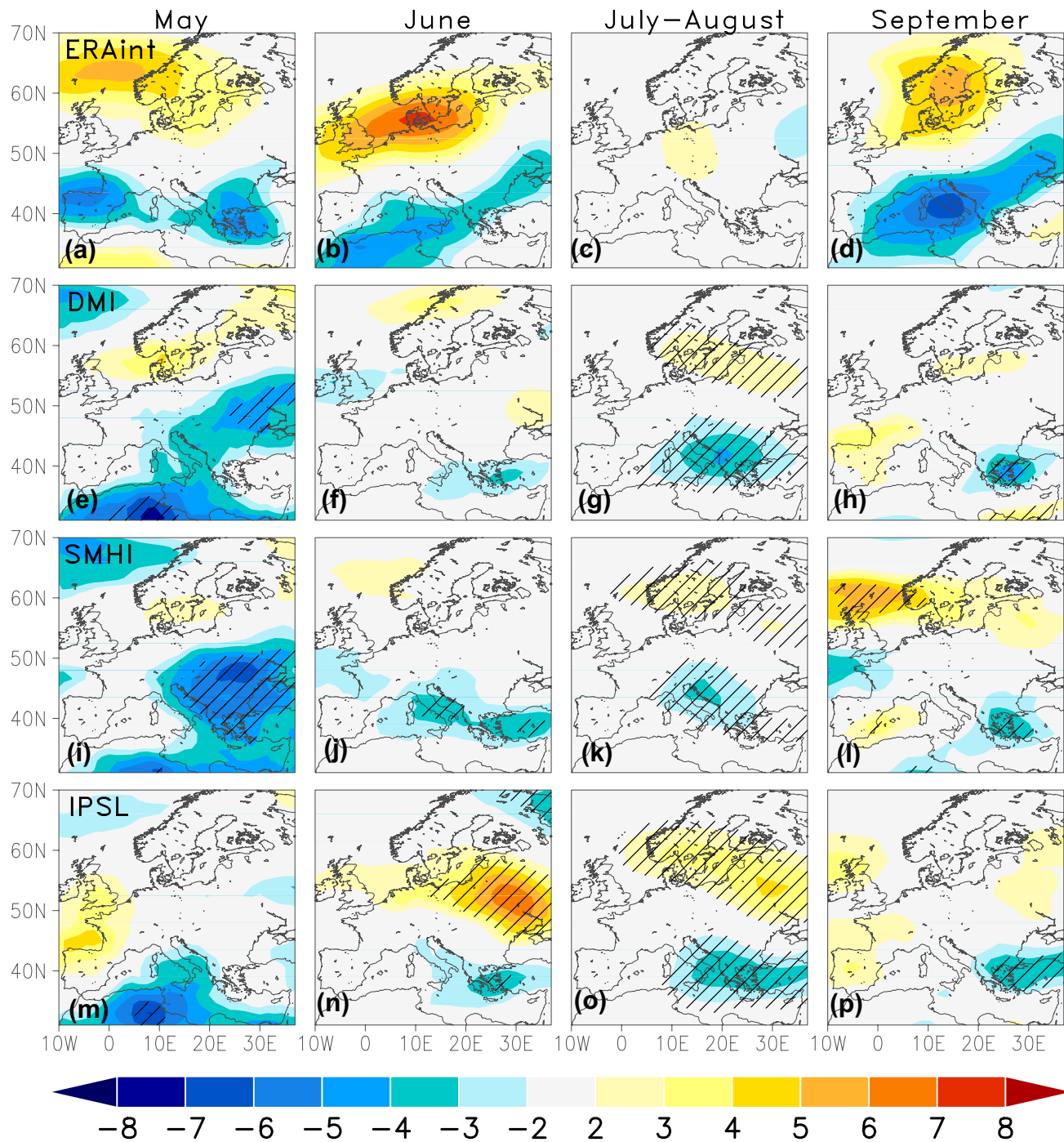
Fig. 8 Mean U200 (m/s) anomaly composites of (**a–d**) ERAint and differences between the (**e–h**) DMI, (**i–l**) SMHI, (**m–p**) IPSL and the ERAint for each subperiod (M,J,JA,S) during the intense Etesian days. U200 anomalies are calculated with respect to the extended summer season of the period 1989–2004. Hatching denotes statistically significant areas at the 95% level

biases are slightly higher (lower) in DMI, SMHI and IPSL (CNRMs) compared to the intense Etesian days, indicating that these models show higher (lower) skill in simulating the extreme wind speeds.

4.6 Taylor diagrams

Figure 9 shows the Taylor diagrams for the mean SLP and Z500 daily anomalies (with respect to May–September of the period 1989–2004) as well as the wind speed of each
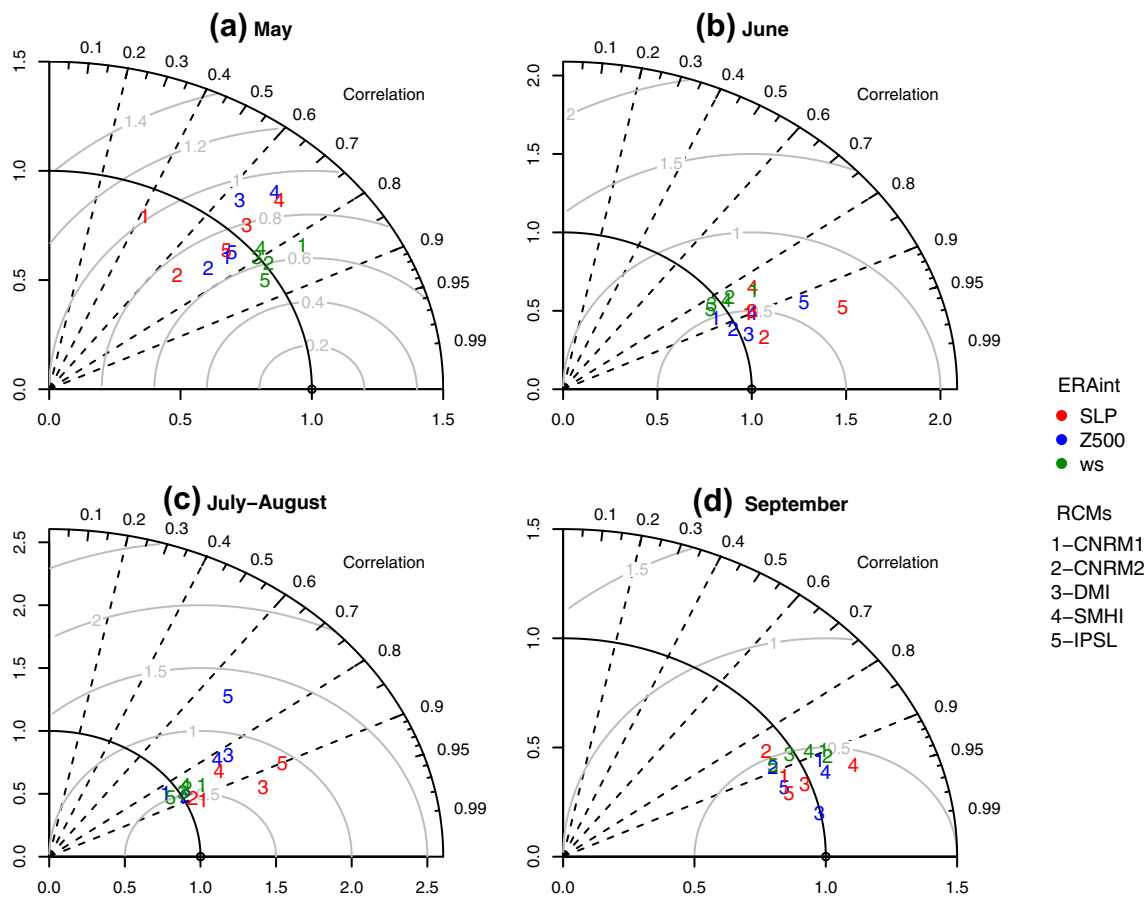
Fig. 9 Taylor diagrams of normalized pattern statistics describing mean spatial variability of SLP anomalies (red), Z500 anomalies (blue) and wind speed (green) from RCMs using ERAint as observing reference within the EURO-CORDEX domain (Fig. 1; left panel)

RCM, with the EURO-CORDEX domain, using the ERAint as a reference.

During May (Fig. 9a), the correlation between models and reanalysis is rather low and ranges between ~0.65–0.75 for the SLP and Z500 anomalies. CNRMs and IPSL provide lower spatial variability than ERAint (with a standard deviation < 1), while its magnitude varies widely among RCMs. The RMSD is in most cases relatively large, about 0.7–1. In June (Fig. 9b), most RCMs simulate the SLP and Z500 anomalies reasonably well, with quite high spatial correlation (higher than 0.9), low RMSD (~0.5) and higher spatial variability than ERAint. CNRM2 shows best skill in these evaluation metrics. During July–August (Fig. 9c), the SLP and Z500 correlation between the models and reanalysis is in most cases about 0.8–0.9. Most of the models provide higher spatial variability than ERAint, while the RMSD is in most cases around 0.5–1; however, model performance varies widely, while CNRMs (DMI and IPSL) generally perform best (worse). All RCMs show good performance in simulating the SLP and Z500 anomalies during September, with spatial pattern correlation coefficients higher than 0.9

and RMSD below 0.5 with respect to the ERAint (Fig. 9d). DMI (CNRM2) in September yields the highest (lowest) pattern correlation and the smallest (highest) RMSD, when evaluated against ERAint. A significant improvement in the RMSD and in the spatial correlation is achieved within the smaller Greek domain for the SLP and Z500 anomalies (see Fig. S10 in SOM). In addition, regarding the wind speed, all models and for all months/subperiods show very low spread, correlation of about 0.8–0.9, RMSD of about 0.5–0.6, while they tend to exhibit spatial variability similar to the ERAint, as reflected by the agreement in standard deviations. Finally, the wind speed exhibits similar behavior in both domains (see Fig. 9 and Fig. S10 in SOM).

The analysis based on ERA20C provides quite similar results for both regions (not shown), while the 20CRv2c indicates generally lower correlations for wind speed (0.7–0.8) and higher spread among the five RCMs for all variables (not shown).

Overall, the RCMs simulate particularly well the mean SLP and Z500 anomalies as well as the wind speed in both regions, with differences depending on the investigated

month. September shows the best performance among the studied months/subperiods.

5 Discussion

This study provides an evaluation of the high spatial resolution hindcast simulations from five RCMs participating in the EURO-CORDEX initiative, with respect to their ability to realistically reproduce the wind field and Etesian days over the Aegean Sea as well as the related large scale atmospheric circulation. The evaluation highlights the general ability of the state-of-the-art RCMs to represent the basic characteristics of the Etesian wind system. Model performance varies according to regions, subperiods and the investigated atmospheric level compared to reanalyses.

All five RCMs show good skills in the simulation of the number of intense Etesian days, although the events are often not synchronized. This behavior can be explained by the lack of model nudging and by the large-scale dynamic response induced by the RCMs within the modeled domain, given the boundary forcing that could lead to intense Etesians. During the observed intense Etesian days not identified in the model simulations, RCMs still show a large-scale atmospheric dipole. However, the two centers of this dipole are misplaced. Nevertheless, all RCMs, but IPSL, are able to capture episodes that are even longer than one week. According to Tyrlis and Lelieveld (2013) the duration of the Etesian episodes is determined by midlatitude dynamics. More specifically, an enhanced and persistent ridge over the central Europe and Balkans can lead to prolonged episodes. Hence, the ability of a model in capturing the long duration episodes demonstrates its skill in reproducing the related dynamical mechanism that controls Etesians' duration.

DMI, SMHI and IPSL show good skill in simulating the wind speed over the Aegean coastal stations, as biases do not exceed ~2 m/s. The best simulation is achieved during the intense Etesian days. The ability of regional climate models to resolve major features of the topography and surface properties (such as coastal boundaries), as well as to develop accurate wind climatology has been also identified in previous studies (Zhang et al. 2012; Salvação et al. 2014). Except for moderate Etesians, wind speed is clearly underestimated in CNRMs. Several studies have also reported a tendency of CNRM1 to underestimate the wind speed over the Adriatic due to the complex orography of the area (Ardhuin et al. 2007; Bertotti and Cavaleri 2009; Sikiric et al. 2015), or to the Gulf of Lion (Obermann et al. 2016) as well as in regions of intense winds, such as the Aegean basin (Herrmann et al. 2011). Further, the RCMs exhibit higher ability in representing the wind direction frequency distribution compared to reanalyses. Global reanalysis limitations in complex terrains (e.g. the Strait of Gibraltar, the Persian Gulf, Ireland)

have been also highlighted in previous studies (Sotillo et al. 2005; Nolan et al. 2011). As shown in Lebassi-Habtezion and Diffenbaugh (2013) and in Salvação et al. (2014), the non-hydrostatic, meso-scale model IPSL shows the best performance regarding wind simulations over land and rough coastal areas.

In agreement with previous studies (Winterfeldt and Weisse 2009; Herrmann et al. 2011 and; Lucas-Picher et al. 2017), high resolution RCMs (except the CNRMs) show an added value in wind speed in areas of complex orography, i.e. along the slopes of the Pindus mountainous range and in coastal areas i.e. over the central and southwestern Aegean stations. A clear added value to the most Etesian-exposed stations (i.e. exposed to the prevailing strongest winds, located mostly over north and central Aegean) can be easily identified in SMHI.

RCM simulations can reproduce the ERA-Interim patterns of the atmospheric circulation associated with intense Etesians both at surface and at 500 hPa when compared to reanalyses. Consistent patterns can be seen at both levels. The RCMs show best (worse) agreement with reanalyses in September (May). All RCMs, demonstrate a general intensification of the high pressure system over central Europe which coexists with an eastward extension of the 500 hPa ridge. The latter partly suppresses the anomalous trough over Turkey and, thus, it results in a weaker anomalous meridional circulation. This phenomenon, which is more pronounced in June for DMI, SMHI and IPSL, could partially explain the underestimation of northerly flow (Etesians) over the Aegean. Model performance improves significantly with decreasing pressure gradient (i.e. during the moderate Etesian days).

Previous studies have noted that the internal variability in an RCM is related to the large-scale weather regime and the model domain size: large (small) domains and weak (strong) flow regimes can lead to large (weak) internal variability (Lucas-Picher et al. 2008b; Laprise et al. 2012). Persistent high pressure systems or blocking patterns have the potential to reduce the model's boundary forcing. The RCM can therefore induce a large-scale atmospheric response not fully coherent with the one given by the driving model/reanalysis (Sieck and Jacob 2016). The Euro-Atlantic region presents higher blocking frequency in May and June, compared to the other examined subperiods (D'Andrea et al. 1998) which may explain the highest differences found in May and June. In addition, the circulation pattern during intense Etesians is dominated by an amplified ridge over central Europe (particularly pronounced in May and June; Dafka et al. 2016).

Nevertheless, shortcomings arise from the large-scale atmospheric circulation in the driving reanalysis are inherited to a certain extent, since near-surface wind speeds are found to exhibit low biases (especially over the Aegean Sea). This is further reinforced if we consider results regarding

the U200 that, albeit with some minor differences, provide confidence that the main processes, driving the jet streams during the intense Etesian days, are faithfully reproduced by the models. Both CNRM simulations which are able to produce large-scale dynamics, given realistic boundary forcing, are unable to simulate extreme wind speeds resulting from these dynamics. This may result from problems related to physical parameterization and the surface schemes and/or issues in regional boundary layer effects.

CNRM2 is the only model, considered in this study that uses a special regional setup, in which the model is strongly relaxed towards ERAInt outside of the EURO-CORDEX domain. This approach may enhance the ability of the model to correctly simulate the chronology of synoptic events and to avoid spurious boundary effects (Kotlarski et al. 2014). Note also that CNRM2 shows the best skill in simulating the Etesian episodes.

Large-scale spectral nudging can reduce the RCM induced large-scale signal and increase the driving field constraint (Alexandru et al. 2009; Herrmann et al. 2011; Berg et al. 2013; Omrani et al. 2013, 2015). A number of studies has shown that spectral nudging can improve the RCM performance in simulating extreme events (Feser and Barcikowska 2012; Otte et al. 2012) and near surface wind speed (Weisse and Feser 2003; Winterfeldt and Weisse 2009; Omrani et al. 2015). Indeed, large-scale nudging may also have positive effects in the simulation of the intense Etesians by "forcing" the RCMs retaining large-scale features. Nevertheless, this study shows that the wind speed, simulated by the RCMs, is to some degree independent from the lateral boundaries conditions, potentially exhibiting greater dependence on the RCM architecture. However, nudging may disrupt the development of the intrinsic smaller-scale features produced by RCMs, not given by the large-scale driving forcing (Cha et al. 2011). This is especially true when RCMs are driven by GCMs (e.g. for climate projections), since nudging might force the RCM to retain and strengthen biases that already exist in GCMs (Pielke et al. 2012).

The validation of RCMs, forced with perfect boundary, is the first necessary step (Giorgi et al. 2001) but not a sufficient for simulating future climate change. GCMs might have biases both in the atmosphere but also in the sea-surface conditions (Hernández-Díaz et al. 2016), that might strongly affect the simulations of the Etesians in the RCMs. Therefore, additional study of RCMs driven by boundary conditions from GCMs should be done, before assessing future projections.

In addition to lateral boundary conditions, RCMs are also influenced by the lower boundary, i.e., properties of sea-surface temperature (SST) and sea ice. Katragkou et al. (2015) highlighted the importance of surface forcing evaluation exercises on RCMs. So far, only few sensitive studies

have explored the dependency of RCM results using higher resolution SSTs (observed) as lower boundary conditions (Chelton et al. 2006; Woollings et al. 2010a; Koltzow et al. 2011). Hernández-Díaz et al. (2016) argued that the mean circulation, the spatial and temporal variability and the position of the jet streams can be improved when observed SSTs are used. This topic deserves further investigation, especially in complex areas such as the Aegean Sea, which is characterized by increased SST variability and upwelling processes during summer due to the Etesians (Kostopoulos and Helmis 2014).

The performance in reproducing extreme wind events is strong, both when only the common and all the intense Etesians are examined. The latter boosts confidence in the ability of these models to simulate the Etesians. We should also note that results are highly dependent on the quality of the observational data used, which is a source of uncertainty in the evaluation process.

6 Conclusions

We assess the performance of EURO-CORDEX RCMs driven by perfect boundary conditions in simulating the Etesians. We further investigate how synoptic circulation biases impact RCMs and influence their ability in simulating the surface wind speed.

This study has shown that the EURO-CORDEX RCMs provide a very good representation of the Etesians over the Aegean, even with a reasonably good percentage of agreement of synchronous events. In some cases, the RCMs (especially DMI, SMHI and IPSL) show a drift from the large-scale circulation patterns of the driving reanalysis. The large scale signal is still captured in those cases, however the dipole is misplaced. Nudging could help to get more synchronous events; but in a GCM-RCM climate projection assessment, this would prevent RCMs to induce changes in the large-scale as a response to regional/local dynamics (better reproduced in principle). This study has confirmed that Etesians are large-scale induced but it has also shown how the interaction with the other smaller scales can trigger these events even without the proper large-scale precondition.

Moreover, DMI, SMHI and IPSL allow for a satisfactory estimation of extreme wind speed over the Aegean, and could be considered as valuable tools for wind energy applications, such as wind site assessment studies. This is especially important in this area which suffers from lack of observations.

Future analysis will be focused on the simulation of Etesians by GCM-RCM runs and their ability to replicate observed variability. New evidence on projected extreme winds for the twenty-first century will be studied, with the

aim to address the potential for wind energy over the Aegean Archipelago.

References

Alexandru A, de Elia R, Laprise R, Separovic L, Biner S (2009) Sensitivity study of regional climate model simulations to large- scale nudging parameters. Mon Weather Rev 137:1666–1686. doi: 10.1175/2008MWR2620.1

Anagnostopoulou C, Zanis P, Katragkou E, Tegoulias I, Tolika K (2014) Recent past and future, patterns of the Etesian winds based on regional scale climate model simulations. Clim Dyn 42:1819–1836. doi: 10.1007/s00382-013-1936-0

Ardhuin F, Bertotti L, Bidlot J-R, Cavaleri L, Filipetto V, Lefevre J-M, Wittmann P (2007) Comparison of wind and wave measurements and models in the Western Mediterranean Sea. Ocean Eng 34:3–4, 526–541

Berg P, Döscher R, Koenigk T (2013) Impacts of using spectral nudging on regional climate model RCA4 simulations of the Arctic. Geosci Model Dev Discuss 6:495–520. doi:10.5194/gmdd-6-495-2013

Berthou S, Mailler S, Drobinski P, Arsouze T, Bastin S, Béranger K, Lebeaupin-Brossier C (2016) Lagged effects of the Mistral wind on heavy precipitation through ocean-atmosphere coupling in the region of Valencia (Spain). Clim Dyn 1–15. doi 10.1007/s00382-016-3153-0

Bertotti L and Cavaleri L (2009) Wind and wave predictions in the Adriatic Sea. J Mar Syst 78:S227–S234. doi:10.1016/j.jmarsys.2009.01.018

Bloom A, Kotroni V, Lagouvardos K (2008) Climate change impact of wind energy availability in the Eastern Mediterranean using the regional climate model PRECIS. Nat Hazards Earth Syst Sci 8:1249–1257

Borhan Y (1998) Mesoscale interactions on wind energy potential in the northern Aegean region: a case study. Renew Sust Energy Rev 2:353–360

Cameron AC, Trivedi PK (1990) Regression-based Tests for overdispersion in the Poisson model. J Econom 46:347–364

Cameron AC, Trivedi PK (1998) Regression Analysis of count data. Cambridge University Press, Cambridge

Cha DH, Jin CS, Lee DK, Kuo YH (2011) Impact of intermittent spectral nudging on regional climate simulation using weather research and forecasting model. J Geophys Res 116:D10103. doi:10.1029/2010JD015069

Chelton DB, Freilich M, Sienkiewicz J, Von Ahn J (2006) On the use of QuikSCAT scatterometer measurements of surface winds for marine weather prediction. Mon Weather Rev 134, 2055–2071. Doi:10.1175/MWR3179.1

Compo GP et al (2011) The twentieth century reanalysis project. Q J R Meteorol Soc 137:1–28

Compo GP, Whitaker JS, Sardeshmukh PD, Giese B, Brohan P (2015) Intercomparison of an improved 20th century reanalysis version "2c" (1850–2012). American Meteorological Society Annual meeting, Phoenix, AZ, January 2015. Presentation

D'Andrea F, Tibaldi S, Blackburn M, Boer G, Deque M, Dix MR, Dugas B, Ferranti L, Iwasaki T, Kitoh A, Pope V, Randall D, Roeckner E, Straus D, Stern W, Van den Dool H, Williamson D (1998) Northern hemisphere atmospheric blocking as simulated by 15 atmospheric general circulation models in the period 1979–1988. Clim Dyn 14(6):385–407. doi:10.1007/s003820050230

Dafka S, Xoplaki E, Toreti A, Zanis P, Tyrlis E, Zerefos C, Luterbacher J (2016) The Etesians: from observations to reanalysis. Clim Dyn 47:1569–1585. doi:10.1007/s00382-015-2920-7

Dee DP et al (2011) The ERA-Interim re-analysis: configuration and performance of the data assimilation system. Q J R Meteorol Soc 137:553–597

Diaconescu EP, Laprise R (2013) Can added value be expected in RCM-simulated large. scales? Clim Dyn 41(7):1769–1800. doi:10.1007/s00382-012-1649-9

Feser F (2015) Climate sciences meet visual arts—the visiting artist researcher experiment. J Sci Commun 14(01):C02

Feser F, Barcikowska M (2012) The influence of spectral nudging on typhoon formation in regional climate models. Environ Res Lett 7 014024. doi:10.1088/1748-9326/7/1/014024

Feser F, Rockel B, von Storch H, Winterfeldt J, Zahn M (2011) Regional climate models add value to global model data—a review and selected examples. Bull Am Meteorol Soc 92:1181–1192. doi:10.1175/2011BAMS3061.1

Fyrippis I, Axaopoulos PJ, Panayiotou G (2010) Wind energy potential assessment in Naxos Island, Greece. Appl Energy 87:577–586

García-Bustamante E, González-Rouco JF, Jiménez PA, Navarro J, Montávez JP (2008) The influence of the Weibull assumption in monthly wind energy estimation. Wind Energy 11:483–502

García-Bustamante E, González-Rouco JF, Jiménez PA, Navarro J, Montávez JP (2009) A comparison of methodologies for monthly wind energy estimation. Wind Energy 12:640–659

Giorgi F et al (2001) Regional climate information - evaluation and projections. Contribution of working group I to the third assessment report of the Intergovernmental Panel on Climate Change. Cambridge University Press, Cambridge, pp 583–638

Giorgi F, Jones C, Asrar GR (2009) Addressing climate information needs at the regional level: the CORDEX framework. Bull World Meteorol Organ 58:175–183

Hernández-Díaz L, Laprise R, Nikiéma O, Winger K (2016) 3-Step dynamical downscaling with empirical correction of sea-surface conditions: application to a CORDEX Africa simulation. Clim Dyn. doi:10.1007/s00382-016-3201-9

Herrmann M, Somot S, Calmanti S, Dubois C, Sevault F (2011) Representation of spatial and temporal variability of daily wind speed and of intense wind events over the Mediterranean Sea using dynamical downscaling: impact of the regional climate model configuration. Nat Hazards Earth Syst Sci 11:1983–2001. doi:10.5194/nhess-11-1983-2011

Iizuka S, Dairaku K, Sasaki W, Adachi SA, Ishizaki NN, Kusaka H, Takayabu I (2012) Assessment of ocean surface winds and tropical cyclones around Japan by RCMs. J Meteorol Soc Jpn 90B:91–102. doi: 10.2151/jmsj.2012-B08

Jacob D et al (2014) Euro-CORDEX: New high-resolution climate change projections for European impact research. Regional Environ Change 14(2):563–578

Joliffe IT, Stephenson DB (2003) Forecast Verification: a practitioner's guide in Atmospheric Science. Wiley, New York

Jones RW, Renfrew A, Orr A, Webber BGM, Holland DM, Lazzara MA (2016) Evaluation of four global reanalysis products using in situ observations in the Amundsen Sea Embayment, Antarctica. J Geophys Res Atmos 121:6240–6257

Kallos G, Kassomenos P, Pielke RA (1993) Synoptic and mesoscale weather conditions during air pollution episodes in Athens, Greece. Bound Layer Meteor 63:163–184

Katragkou E, García-Díez M, Vautard R, Sobolowski S, Zanis P, Alexandri G, Cardoso RM, Colette A, Fernandez J, Gobiet A, Goergen K, Karacostas T, Knist S, Mayer S, Soares PMM, Pytharoulis I, Tegoulias I, Tsikerdekis A, Jacob D (2015) Regional climate hindcast simulations within EURO-CORDEX: evaluation of a WRF multi-physics ensemble. Geosci Model Dev 8:603–618

Kent EC, Fangohr S, Berry DI (2013) A comparative assessment of monthly mean wind speed products over the global ocean. Int J Clim 33(11):2520–2541. doi:10.1002/joc.3606

Koltzow MAO, Iversen T, Haugen JE (2011) The importance of lateral boundaries, surface forcing and choice of domain size for dynamical downscaling of global climate simulations. Atmosphere 2:67–95

Kostopoulos V, Helmis C (2014) Flux measurements in the surface marine atmospheric boundary layer over the Aegean Sea, Greece. Sci Total Env 494–495: 166–176. doi:10.1016/j.scitotenv.2014.06.127

Kotlarski S, Keuler K, Christensen OB, Colette A, Déqué M, Gobiet A, Goergen K, Jacob D, Lüthi D, van Meijgaard E, Nikulin G, Schär C, Teichmann C, Vautard R, Warrach-Sagi K, Wulfmeyer V (2014) Regional climate modeling on European scales: a joint standard evaluation of the EURO-CORDEX RCM ensemble. Geosci Model Dev 7:1297–1333. doi: 10.5194/gmd-7-1297-2014

Kunz M, Mohr S, Rauthe M, Lux R, Kottmeier C (2010) Assessment of extreme wind speeds from regional climate models-part 1: estimation of return values and their evaluation. Nat Hazards Earth Syst Sci 10:907–922. doi:10.5194/nhess-10-907-2010

Laprise R, Kornic D, Rapaic M, Separovic L, Leduc M, Nikiema O, Luca AD, Diaconescu E, Alexandru A, Lucas-Picher P, de Elia R, Caya D, Biner S (2012) Climate change, chapter considerations of domain size and large-scale driving for nested regional climate models: impact on internal variability and ability at developing small-scale details, p 244. Springer, Wien

Lebassi-Habtezion B, Diffenbaugh NS (2013) Nonhydrostatic nested climate modeling: a case study of the 2010 summer season over the western United States. J Geophys Res Atmos 118, 10,944–10, 962

Lebeaupin-Brossier C, Béranger K, Deltel C, Drobinski P (2011) The Mediterranean response to different space-time resolution atmospheric forcings using perpetual mode sensitivity simulations. Ocean Model 36:1–25. doi:10.1016/j.ocemod.2010.10.008

Lucas-Picher P, Caya D, de Elia R, Laprise R (2008b) Investigation of regional climate models' internal variability with a ten-member ensemble of 10- year simulations over a large domain. Clim Dyn 31(7–8):927–940. doi: 10.1007/s00382-008-0384-8

Lucas-Picher P, Laprise R, Winger K (2017) Evidence of added value in North American regional climate model hindcast simulations using ever-increasing horizontal resolutions. Clim Dyn 2611:2633. doi 10.1007/s00382-016-3227-z

Menut L, Tripathi OP, Colette A, Vautard R, Flaounas E, Bessagnet B (2013) Evaluation of regional climate simulations for air quality modeling purposes. Clim Dyn. doi:10.1007/s00382-012-1345-9

Metaxas DA, Bartzokas A (1994) Pressure covariability over the Atlantic, Europe and N. Africa. Application: centers of action for temperature, winter precipitation and summer winds in Athens, Greece. Theor Appl Climatol 49:9–18

Nabat P, Somot S, Mallet M, Sevault F, Chiacchio M, Wild M (2015) Direct and semi-direct aerosol radiative effect on the Mediterranean climate variability using a regional climate system model. Clim Dyn. doi:10.1007/s00382-014-2205-6

Nikulin G, Kjellstrom E, Hansson U, Strandberg G, Ullerstig A (2011) Evaluation and future projections of temperature, precipitation and wind extremes over Europe in an ensemble of regional climate simulations. Tellus A 63:41–55

Nolan P, Lynch P, McGrath R, Semmler T, Wang S (2011) Simulating climate change and its effects on the wind energy resource of Ireland. Wind Energy 15:593–608

Obermann A, Bastin S, Belamari S, Conte D, Gaertner MA, Li L, Ahrens B (2016) Mistral and tramontane wind speed and wind direction patterns in regional climate simulations. Clim Dyn 1–18. doi:10.1007/s00382-016-3053-3

Omrani H, Drobinski P, Dubos T (2013) Optimal nudging strategies in regional climate modelling: investigation in a big-brother experiment over the European and Mediterranean regions. Clim Dyn 41:2451–2470. doi:10.1007/s00382-012-1615-6

Omrani H, Drobinski P, Dubos T (2015) Using nudging to improve global-regional dynamic consistency in limited-area climate modeling: what should we nudge? Clim Dyn 44:1627–1644. doi: 10.1007/s00382-014-2453-5

Otte TL, Nolte CG, Otte MJ, Bowden JH (2012) Does nudging squelch the extremes in regional climate modeling? J Climate 25:7046–7066. doi:10.1175/JCLI-D-12-00048.1

Pezzoli A (2005) Observation and analysis of etesian wind storms in the Saroniko Gulf. Ad Geo 2:187–194. doi:10.5194/adgeo-2-187-2005

Pielke RA, Wilby R, Niyogi D, Hossain F, Dairuku K, Adegoke J, Kallos G, Seastedt T, Suding K (2012) Dealing with complexity and extreme events using a bottom-up, resource-based vulnerability perspective, in extreme events and natural hazards: the complexity perspective. American Geophysical Union, Washington D.C. doi:10.1029/2011GM001086

Poli P, Hersbach H, Tan D, Dee D, Thépaut J-N, Simmons A, Peubey C, Laloyaux P, Komori T, Berrisford P, Dragani R, Trémolet Y, Holm E, Bonavita M, Isaksen L, Fisher M (2013) The data assimilation system and initial performance evaluation of the ECMWF pilot reanalysis of the 20th-century assimilating surface observations only (ERA-20C). ERA Report Series no. 14, ECMWF, pp. 59

Prein AF, Gobiet A, Truhetz H, Keuler K, Goergen K, Teichmann C, Fox Maule C, van Meijgaard E, Déqué M, Nikulin G, Vautard R, Colette A, Kjellström E, Jacob D (2016) Precipitation in the EURO-CORDEX 0.11° and 0.44° simulations: high resolution, high benefits?. Clim Dyn. doi:10.1007/s00382-015-2589-y

Pryor SC and Barthelmie RJ (2011) Assessing climate change impacts on the near-term stability of the wind energy resource over the USA. Proc Natl Acad Sci USA. 108:8167–8171. doi:10.1073/pnas.1019388108

Räisänen J, Hansson U, Ullerstig A, Döscher R, Graham LP et al. (2004) European climate in the late twenty-first century: regional simulations with two driving global models and two forcing scenarios. Clim Dyn 22:13–31

Rockel B, Woth K (2007) Extremes of near-surface wind speed over Europe and their future changes as estimated from an ensemble of RCM simulations. Clim Change 81:267–280

Rummukainen M (2010) State-of-the-art with regional climate models. WIREs Clim Change 1:82–96. doi:10.1002/wcc.8

Rummukainen M, Rockel B, Bärring L, Christensen JH, Reckermann M (2015) Twenty-first-century challenges in regional climate modeling. Bull Amer Meteor Soc 96:ES135-ES138

Salvação N, Bernardino M, Guedes Soares C (2014) Assessing mesoscale wind simulations in different environments. Comput Geosci 71:28–36

Schwierz C, Heck P, Zenklusen E, Bresch DN, Vidale P-L, Wild M, Schär C (2009) Modelling European winter wind storm losses in current and future climate. Clim Change 101:485–514. DOI 10.1007/s10584-009-9712-1

Sieck K, Jacob D (2016) Influence of the boundary forcing on the internal variability of a regional climate model. Am J Clim Change 5:373–382. doi:10.4236/ajcc.2016.53028

Sikiric DM, Janekovic I, Tomazic I, Kuzmic M, Roland A (2015) Comparison of ALADIN and IFS model wind speeds over the Adriatic. Acta Adriat 1(0001–5113):56 67–82

Sotillo M, Ratsimandresy A, Carretero J, Bentamy A, Valero F, Gonzalez-Rouco F (2005) A high-resolution 44-year atmospheric hindcast for the Mediterranean Basin: contribution to the regional improvement of global reanalysis. Clim Dyn 25:219–236

Strandberg G, Bärring L, Hansson U, Jansson C, Jones C, Kjellström E et al. (2014) CORDEX scenarios for Europe from the Rossby Centre regional climate model RCA4. Reports Meteorology and Climatology 116. SMHI, SE-60176 Norrköping, Sverige

Taylor KE (2001) Summarizing multiple aspects of model performance in a single diagram. J Geophys Res 106:7183–7192

Taylor KE, Stouffer RJ and. Meehl GA (2012) An overview of CMIP5 and the experiment design. Bull Am Meteorol Soc 93(4):485–498

Tölle MH, Gutjahr O, Busch G, Thiele JC (2014) Increasing bioenergy production on arable land: Does the regional and local climate respond? Germany as a case study. J Geophys Res Atmos 119:2711–2724

Tyrlis E, Lelieveld J (2013) Climatology and dynamics of the summer Etesian winds over the eastern Mediterranean. J Atmos Sci 70:3374–3396. doi:10.1175/JAS-D-13-035.1

Tyrlis E, Tymvios FS, Giannakopoulos C and Lelieveld J (2015) The role of blocking in the summer 2014 collapse of Etesians over the eastern Mediterranean. J Geophys Res Atmos 120. *doi*:10.1002/2015JD023543

Voldoire A, Sanchez-Gomez E, Salas y Mélia D et al (2013) The CNRM-CM5.1 global climate model: description and basic evaluation. Clim Dyn 40(9):2091–2121. doi:10.1007/s00382-011-1259-y

Weisse R, Feser F (2003) Evaluation of a method to reduce uncertainty in wind hindcasts performed with regional atmosphere models. Coastal Eng 48:211–225

Weisse R, von Storch H, Feser F (2005) Northeast Atlantic and North Sea storminess as simulated by a regional climate model during 1958–2001 and comparison with observations. J Clim 18:465–479

Wilks SS (1962) Mathematical Statistics. Wiley, New York

Winterfeldt J, Weisse R (2009) Assessment of value added for surface marine wind speed obtained from two regional climate models (RCMs). Mon Weather Rev 137(9):2955–2965. doi:10.1175/2009MWR2704.1

Woollings T, Hoskins B, Blackburn M, Hassell D, Hodges K (2010a) Storm track sensitivity to sea surface temperature resolution in a regional atmosphere model. Clim Dyn 35:341–353

Zerefos C (1978) Surface wind energy density over eastern Greece. Arch Met Geoph Biokl Ser B 26:81–86

Zhang C, Wang Y, Lauer A, Hamilton K (2012) Configuration and evaluation of the WRF model for the Study of Hawaiian Regional Climate. Mon Weather Rev. doi:10.1175/MWR-D-11-00260.1